Electronic Supplementary Information

Determination of the electronic structure of a dinuclear dysprosium single molecule magnet without symmetry idealization

Mauro Perfetti[a,†,$], Maren Gysler[a,†], Yvonne Rechkemmer-Patalen[a], Peng Zhang[a], Hatice Taştan[a], Florian Fischer[a], Julia Netz[a], Wolfgang Frey[b], Lucas W. Zimmermann[c], Thomas Schleid[c], Michael Hakl[d], Milan Orlita[d,e], Liviu Ungur[f], Liviu Chibotaru[f], Theis Brock-Nannestad[g], Stergios Piligkos[g], Joris van Slageren[a,*]

[a.] *Institut für Physikalische Chemie, Universität Stuttgart, Pfaffenwaldring 55, D-70569 Stuttgart, Germany.*
[b.] *Institut für Organische Chemie, Universität Stuttgart, Pfaffenwaldring 55, D-70569 Stuttgart, Germany.*
[c.] *Institut für Anorganische Chemie, Universität Stuttgart, Pfaffenwaldring 55, D-70569 Stuttgart, Germany.*
[d.] *Laboratoire National des Champs Magnétiques Intenses (LNCMI-EMFL), CNRS, UGA, 38042 Grenoble, France.*
[e.] *Institute of Physics, Charles University, Ke Karlovu 5, 12116 Praja 2, Czech Republic.*
[f.] *Theory of Nanomaterials Group, Katholieke Universiteit Leuven, Celestijnenlaan 220F, 3001 Leuven, Belgium.*
[g.] *Department of Chemistry, University of Copenhagen, Universitetsparken 5, 2100, Denmark*
[$] *Current address: Department of Chemistry, University of Copenhagen, Universitetsparken 5, 2100, Denmark*
† These authors contributed equally.

Summary

Synthesis

1. General

$[Dy(fod)_3]$ (Alfa Aesar, 98+ %), $[Gd(fod)_3]$ (Alfa Aesar, 98+ %), $Y(NO_3)_3 \cdot 6\ H_2O$ (Sigma Aldrich, 99.8 %), 2,2'-bipyrimidine (Alfa Aesar, 98%), KOH (Alfa Aesar, p.a.), absolute ethanol (VWR, 99.5%), n-hexane (Sigma Aldrich, 98%), dichloromethane (Alfa Aesar, 98%) and diethyl ether (Alfa Aesar, 98%) were used as received. All reactions were carried out in standard glassware under ambient atmosphere.

2. $[Dy_2$(6,6,7,7,8,8,8-Heptafluoro-2,2-dimethyl-3,5-octanedionate)$_6$(μ-2,2'-bipyrimidine)]

To a solution of $Dy(fod)_3$ (0.120 g; 0.115 mmol) in 20 mL absolute ethanol was slowly added a solution of bpm (0.009 g; 0.057 mmol) in 8 mL absolute ethanol. The reaction mixture was stirred at ambient temperature for 3 hours. Slow evaporation of the solvent led to the formation of crystals which were recrystallized from ethanol to give the colorless product in 96% yield. Elemental analysis: found (calc. for $Dy_2C_{68}H_{66}F_{42}N_4O_{12}$)/%: C 36.23 (36.38), H 2.95 (3.08), N 2.49 (2.58). ATR-IR: $\tilde{\nu}_{max}$ = 2969 (bw), 1615 (vs), 1578 (m), 1539 (w), 1507 (m), 1471 (m), 1412 (w), 1345 (s), 1280 (w), 1222 (s), 1152 (s), 1120 (vs), 1104 (s), 1071 (s), 1021 (m), 966 (m), 940 (m), 910 (m), 832 (m), 793 (m), 755 (m), 740 (m), 687 (m), 663 (m) cm^{-1}. ESI-MS: (positive): *m/z* = 2277.2 $[M+Na]^+$; 2117.3 $[[Dy(fod)_6(\mu\text{-bpm})]+Na]^+$; 1959.2 $[[Dy(fod)_6]+Na]^+$; 1526.2 $[[Dy(fod)_4(bpm)]+Na]^+$; 1230.1 $[Dy_2(fod)_2(bpm)_2]^+$; 1070.2 $[Dy(fod)_2(bpm)_2]^+$; 912.1 $[Dy(fod)_2(bpm)]^+$; 504.1 $[[Dy(fod)]+2Na]^+$. ^{1}H-NMR (500 MHz, $CDCl_3$); –13.21 ppm (b), –0.75 ppm (s), 1.21 ppm (s), 7.26 ppm (s),7.34 ppm (s).

3. 4% Dy @ $[Y_2$(6,6,7,7,8,8,8-Heptafluoro-2,2-dimethyl-3,5-octanedionate)$_6$(μ-2,2'-bipyrimidine)]

Same procedure to obtain Dy_2. The starting Ln salt was a mixture of $Dy(fod)_3$:$Y(fod)_3$=1:19. Elemental analysis: found (calc. for $Y_{0.96}Dy_{0.04}C_{68}H_{66}F_{42}N_4O_{12}$)/%: C 38.40 (38.65), H 3.27 (3.14), N 2.80 (2.65).

4. Crystallographic data and refinement parameters for **Dy_2**

Table S1. Crystallographic data and refinement parameters for **Dy_2**.

Formula	$Dy_2C_{68}H_{66}F_{42}N_4O_{12}$
M_r	2254.25
T / K	100(2)
Crystal system	Triclinic
Space group	P-1
a / Å	11. 7327(10)
b / Å	13.5801(12)
c / Å	14.5983(12)
α / °	71.026(4)
β / °	88.785(4)
γ / °	77.839(4)
V / Å^3	2147.4(3)
Z	1
ρ_{calc} / $g\ cm^{-3}$	1.743
μ(Mo-Kα)/mm^{-1}	1.875
F_{000}	1108
Crystal size / mm^3	0.44 x 0.23 x 0.084
Radiation	0.71073 Å
theta range / °	1.624 to 28.321
Reflection collected	36989
Independent reflections	10481
R_{int}	0.0321
Param restraints	658/386
S (on F^2)	1.093
R1, wR2 ($I \geq 2\sigma(I)$)	0.0751, 0.1896
R1, wR2 (all data)	0.0948, 0.1996

5. Powder diffraction

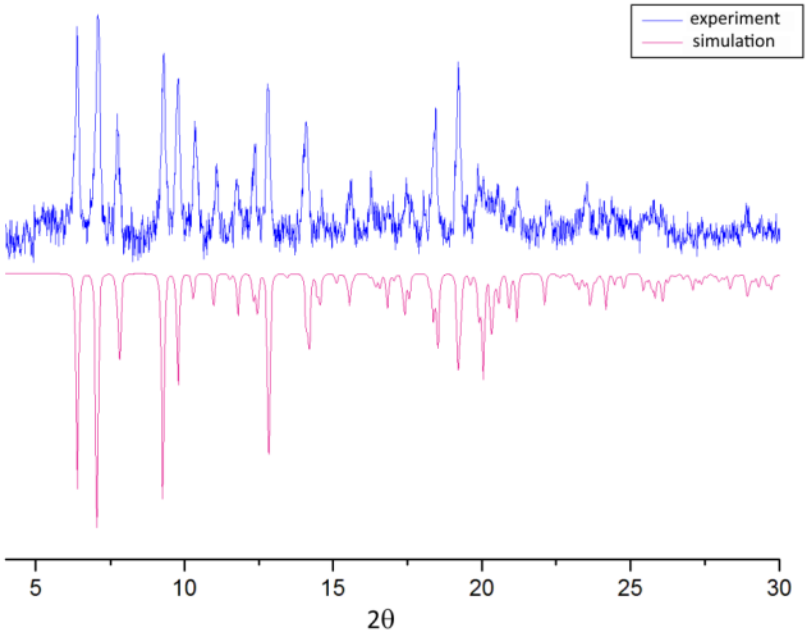

Figure S1. Powder diffractogram of **Dy_2**.

Shape calculation

Table S2. Continuous shape measurements[1] for compound **Dy_2**. The CShM parameter represent the deviation from the ideal shape. Numbers below 2 are usually considered acceptable for a symmetry approximation.

Shape	Symmetry	CShM
Octagon	D8h	33.802
Heptagonal pyramid	C7v	21.534
Hexagonal bipyramid	D6h	17.894
Cube	Oh	17.221
Square antiprism	D4d	17.779
Triangular dodecahedron	D2d	16.286
Johnson gyrobifastigium J26	D2d	18.729
Johnson elongated triangular bipyramid J14	D3h	23.836
Biaugmented trigonal prism J50	C2v	18.226
Biaugmented trigonal prism	C2v	16.011
Snub diphenoid J84	D2d	19.570
Triakis tetrahedron	Td	16.091
Elongated trigonal bipyramid	D3h	24.919

Ab initio calculations

Table S3. Energies (first column), effective *g* tensors (second to forth column), angle between the z axis of each KD and the Dy-Dy axis (fifth column) and angle between the z axis of the ground KD and the z axis of the other KDs (sixth column). An effective $S = 1/2$ is assumed.

E (cm^{-1})	g_x	g_y	g_z	α (°)	β (°)
0	0.01	0.01	19.55	83	-
150	0.26	0.39	16.09	79	8
226	1.07	1.51	13.06	87	36
273	1.90	4.40	9.41	97	148
318	2.87	5.24	8.01	130	89
353	1.53	3.52	16.08	128	111
461	0.02	0.12	18.14	142	85
544	0.02	0.07	19.18	139	57

Table S4. Calculated CF parameters expressed in Wybourne notation.

k	*q*	Ab initio
2	0	592
	1	176
	-1	76
	2	-192
	-2	-93
4	0	588
	1	-63
	-1	164
	2	1
	-2	-538
	3	-138
	-3	337
	4	44
	-4	151
6	0	0
	1	155
	-1	215
	2	136
	-2	-30
	3	151
	-3	-38
	4	-234
	-4	55
	5	53
	-5	-12
	6	-20
	-6	-153

Table S5. CF strength of the calculated CF parameters. We used the following notation: $S_k = \sqrt{\frac{1}{2k+1}(\left|B_k^0\right|^2 + 2 * \sum_{q\neq 0}\left|B_k^q\right|^2)}$ and $S_{tot} = (S_2 + S_4 + S_6)/3$.

	Ab initio/cm^{-1}
S_2	321
S_4	380
S_6	175
S_t	292

Table S6. Energies and composition calculated for the KDs of the ground J=15/2 multiplet of **Dy_2**. We only report contributions >1%.

Dy_2	Energy / cm^{-1}							
	0	150	226	273	318	353	461	544
m_j	$\|1_{CF};\pm\rangle$	$\|2_{CF};\pm\rangle$	$\|3_{CF};\pm\rangle$	$\|4_{CF};\pm\rangle$	$\|5_{CF};\pm\rangle$	$\|6_{CF};\pm\rangle$	$\|7_{CF};\pm\rangle$	$\|8_{CF};\pm\rangle$
±15/2	96%		3%	1%				2%
±13/2		80%	5%	2%	2%	1%	2%	8%
±11/2	2%	3%	38%	25%	3%	1%	6%	19%
±9/2		11%	10%	24%	19%	4%	7%	25%
±7/2	1%	2%	16%	3%	31%	21%	5%	22%
±5/2		2%	9%	12%	4%	47%	11%	15%
±3/2		1%	12%	7%	23%	21%	29%	7%
±1/2			7%	25%	18%	6%	41%	2%

Magnetic Characterization

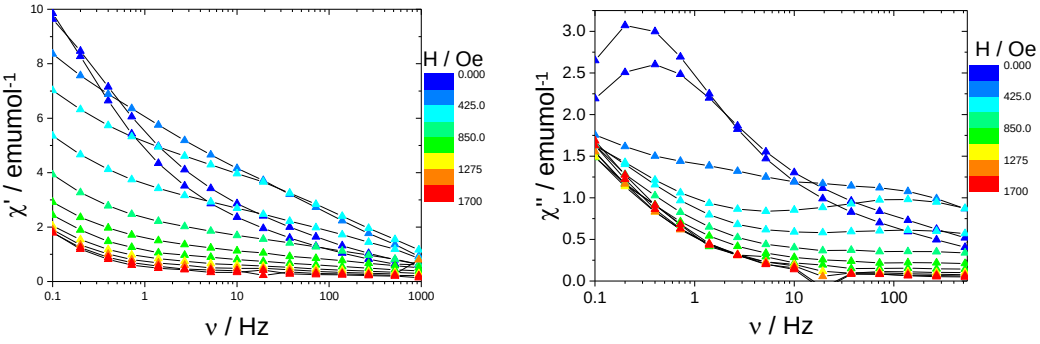

Figure S2. Real (left) and imaginary (right) part of the ac susceptibility of **Dy_2**. Scan field, *T* = 1.8 K.

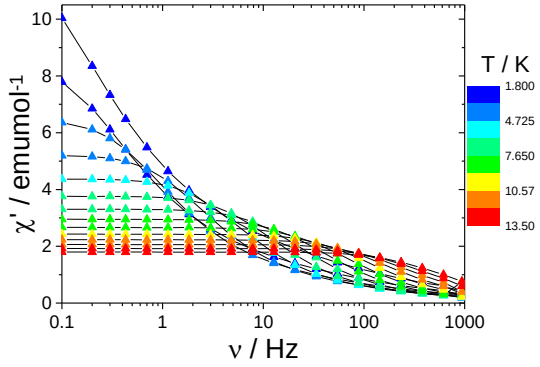

Figure S3. Real part of the ac susceptibility of **Dy_2**. Scan Temperature, *B* = 0 T.

The imaginary part of the magnetic susceptibility was fitted using the Cole-Cole equation[2]:

$$\chi''(\nu) = (\chi_T - \chi_S)\frac{(2\pi\nu\tau)^{1-\alpha}\cos(\pi\alpha/2)}{1+2(2\pi\nu\tau)^{1-\alpha}\sin\left(\frac{\pi\alpha}{2}\right)+(2\pi\nu\tau)^{2-2\alpha}} \qquad (1)$$

Where α is the width of the distribution of the relaxation times, centred at τ. The difference between the thermal and adiabatic susceptibility (χ_T- χ_S) accounts for the fraction of the sample that is following the relaxation pathway. To fit the imaginary susceptibility of **Dy_2** in zero field, we have used a sum of two Cole Cole equations for the low temperature region (*T* < 5 K) while only one process satisfactorily reproduced the data at higher temperature.

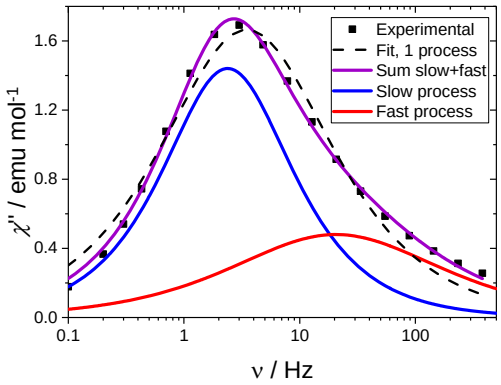

Figure S4. Sample fit of the imaginary part of the susceptibility at *T* = 4.5 K and *B* = 0 T for **Dy_2**. The dashed curve is a fit using a single Cole-Cole function (clearly unsatisfactory). The violet curve is the sum of two (blue and red) Cole-Cole functions.

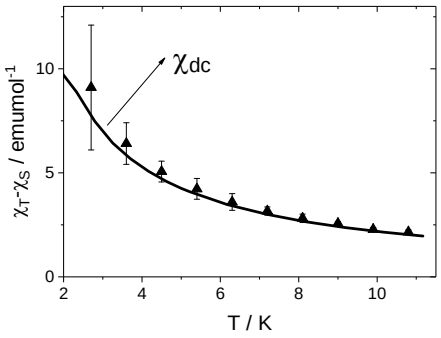

Figure S5. χ_T-χ_S values (symbols, B = 0 T) extracted by the χ'' curves compared with the χ_{dc} values (straight line, B = 0.1 T) in the same temperature range. At T < 5 K the χ_T-χ_S values reported here are the sum of the values relative to the two processes while at higher temperature they are extracted using a single process. A good agreement between ac and dc values means that all the magnetic moments are slowly relaxing.

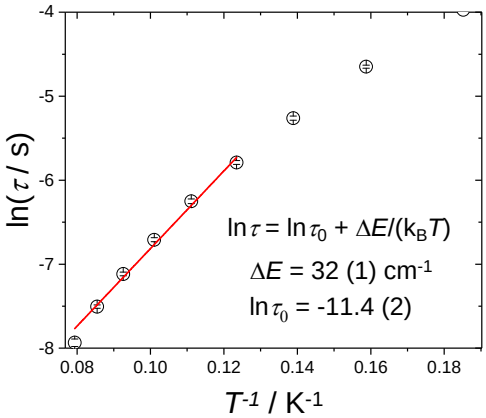

Figure S6. Fit of the high temperature relaxation times using an effective energy barrier (single Orbach process). The extracted value of 32 cm^{-1} is not compatible with both theory or experiments.

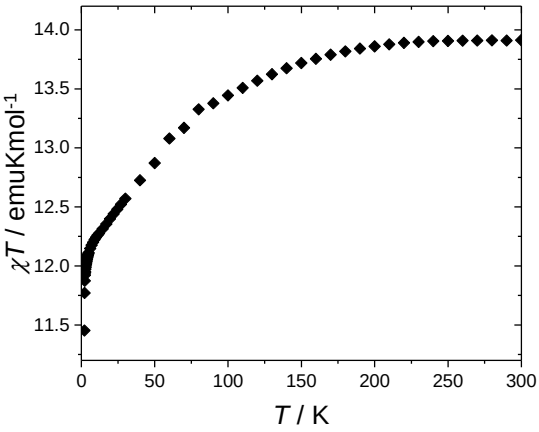

Figure S7. Product of the magnetic dc susceptibility and temperature for Dy@$\mathbf{Y_2}$. The data were corrected for diamagnetism using Pascal's tables and scaled per mole of Dy.

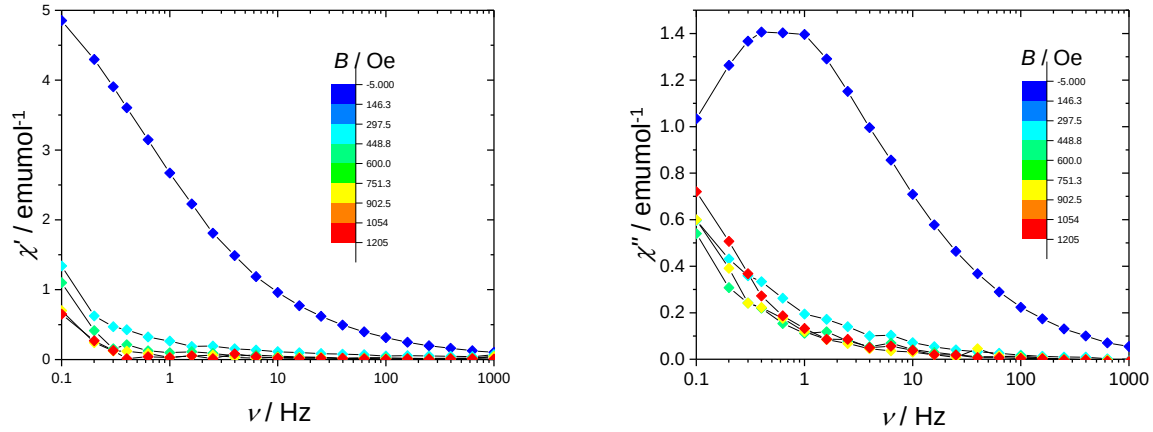

Figure S8. Real (left) and imaginary (right) part of the ac susceptibility of Dy@**Y_2**. Scan Field, T = 1.8 K.

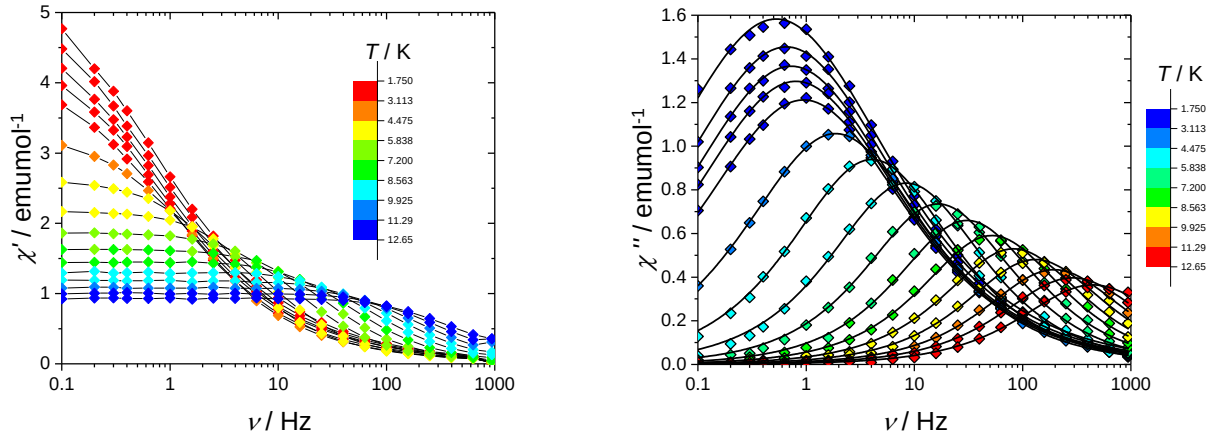

Figure S9. Real (left) and imaginary (right) part of the ac susceptibility of Dy@**Y_2**. Scan Temperature, B = 0 T. Black lines in the χ' graph represent the best fit discussed in the main text.

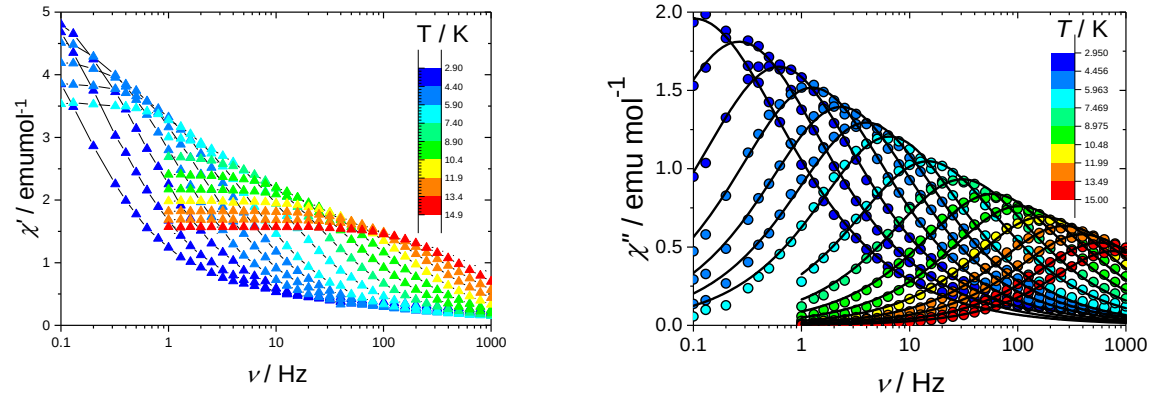

Figure S10. Real (left) and imaginary (right) part of the ac susceptibility of **Dy_2**. Scan Temperature, B = 0.1 T. Black lines in the χ' graph represent the best fit discussed in the main text.

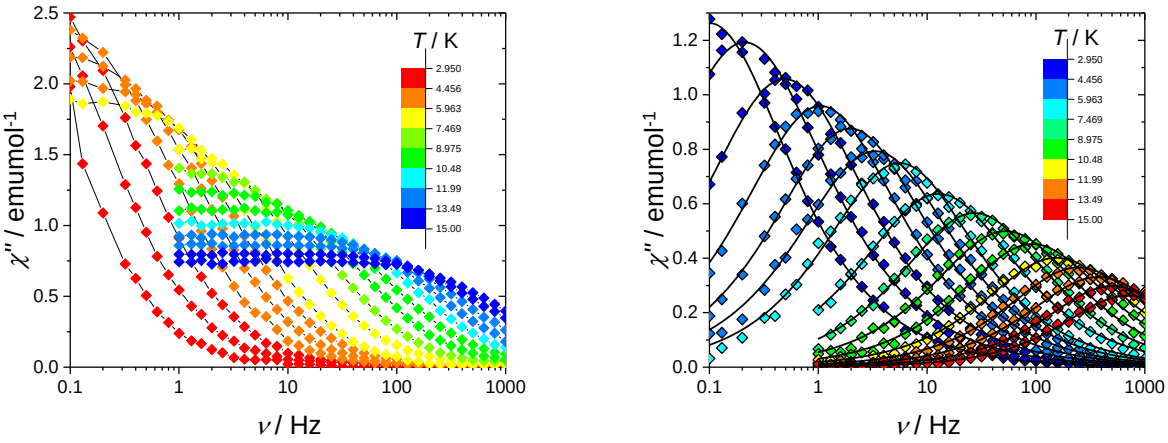

Figure S11. Real (left) and imaginary (right) part of the ac susceptibility of Dy@**Y$_2$**. Scan Temperature, B = 0.1 T. Black lines in the χ'' graph represent the best fit discussed in the main text.

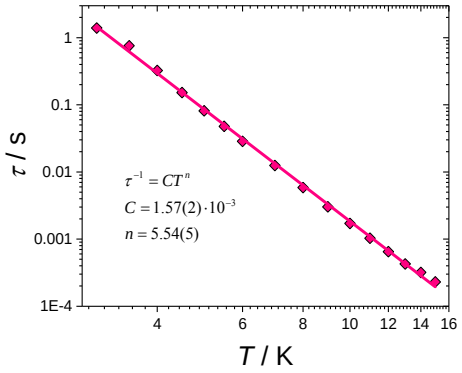

Figure S12. Fit of the relaxation time extracted from the χ'' curves in Fig. S11 for Dy@**Y$_2$**.

Luminescence

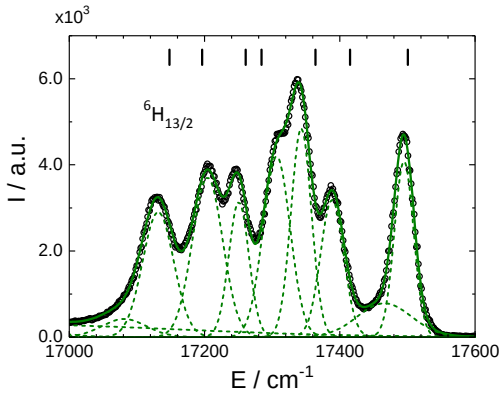

Figure S13. Luminescence spectra corresponding to the transition $^4F_{9/2}$ ->$^6H_{13/2}$.

Ab initio energy scaling

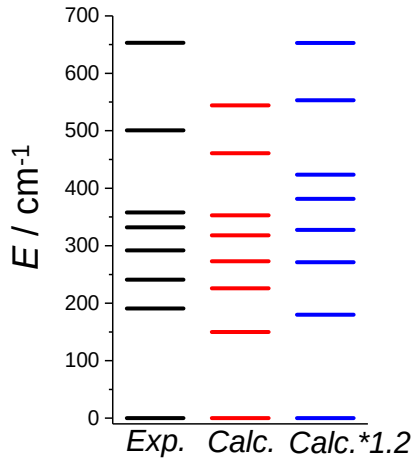

Figure S14. Comparison between experimental energies and calculated energies for the ground $^{6}H_{15/2}$ multiplet of Dy^{3+}. Black lines represent the experiments, red lines the energies calculated *ab initio* and the blue lines the calculated energies scaled for a factor 1.2 to match the total splitting of the multiplet.

Far InfraRed spectroscopy

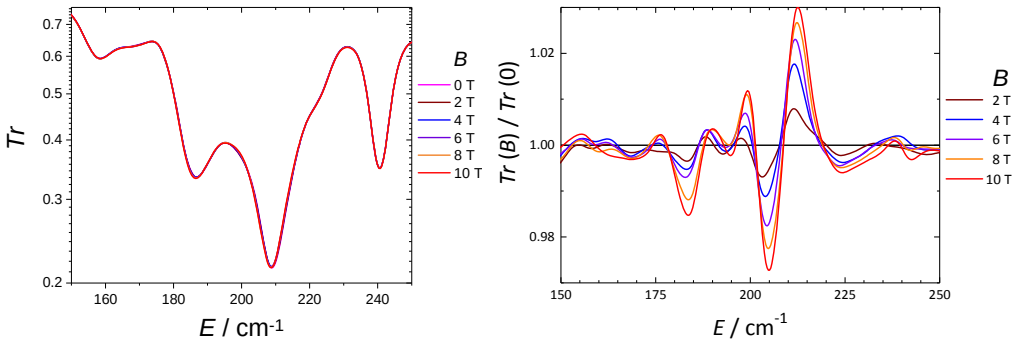

Figure S15. FIR spectra recorded for **Dy_2**. Left: Absolute transmission, Right: Transmission normalized for B = 0 T.

Magnetic Circular Dichroism Spectroscopy

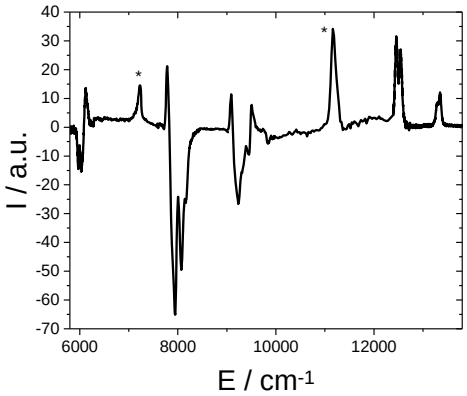

Figure S16. MCD signal recorded at T = 1.6 K and B = ± 2 T. The peaks labelled with a star are instrumental.

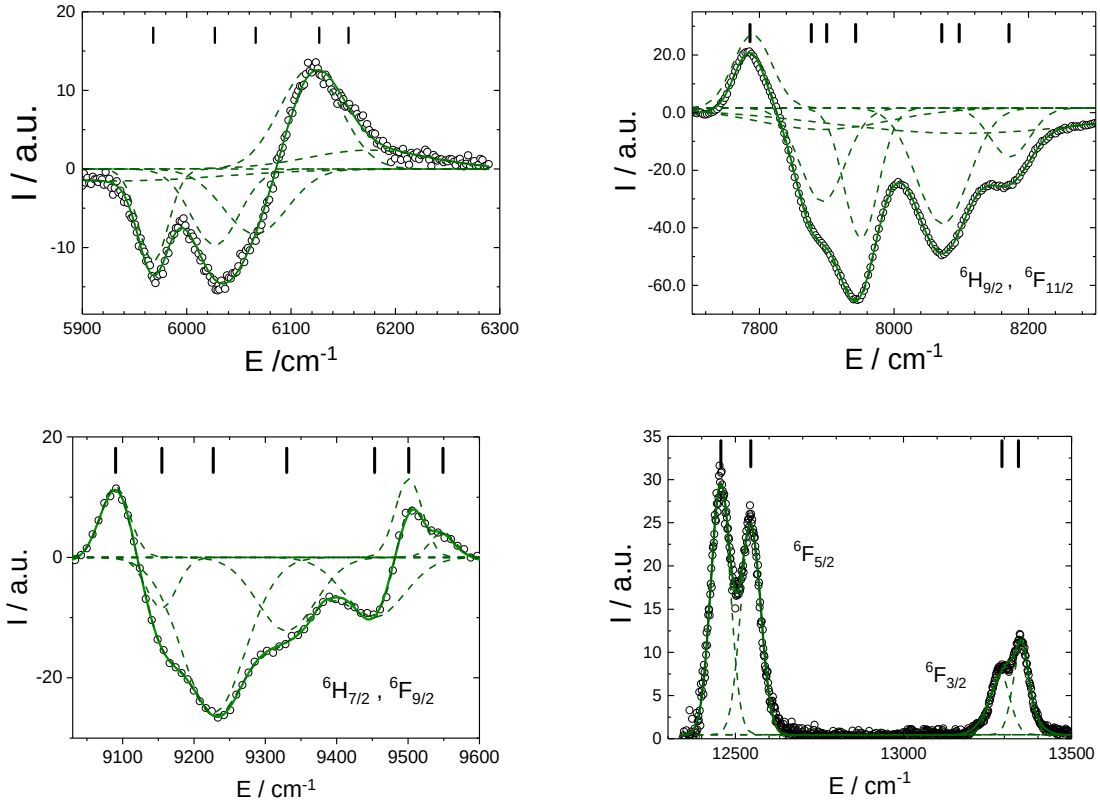

Figure S17. Zoom on the MCD signals relative to the excited multiplets. The green line is the fit obtained as a sum of gaussians. Black ticks are the positions of the extracted energy levels.

Experimental energies

Table S7. Energies extracted from luminescence and MCD experiments.

Spectroscopic term	E (cm^{-1})
$^6H_{15/2}$ complete	0
	191
	241
	292
	332
	358
	501
	653
$^6H_{13/2}$ complete	3577
	3682
	3732
	3768
	3821
	3867
	3942
$^6H_{11/2}$ partial9	5968
	6027
	6066
	6127
	6155
$^6H_{9/2}$ & $^6F_{11/2}$ partial	7786
	7877
	7900
	7943
	8071
	8097

	8171
$^6H_{7/2}$ & $^6F_{9/2}$ partial	9090
	9155
	9227
	9330
	9453
	9501
	9549
$^6F_{5/2}$ partial	12457
	12546
$^6F_{3/2}$ complete	13293
	13342

Crystal Field fitting

Table S8. Single ion parameters extracted from the fit of spectroscopic data.

	Fit
E_{ave}	54763
F_2	85364
F_4	75702
F_6	43023
ζ_{SO}	1879

Table S9. CF parameters extracted from the fit of spectroscopic data under assumption of different CF symmetries.

Param.	D_{4d}		D_{6h}		D_{2d}		C_{2v}		C_1	
	Value	Std dev	Value	Std dev	Value	Std dev	Value	Std dev	Value	Std dev
B_{20}	669	46	657	61	637	53	503	7	511	16
B_{40}	1568	134	1286	214	495	142	1346	44	888	59
B_{60}	1286	198	855	176	-348	182	110	50	-97	114
B_{21}									205	30
B_{2-1}									-131	39
B_{22}							-290	$> 10^4$	99	25
B_{2-2}							42	$> 10^4$	74	26
B_{41}									-510	82
B_{4-1}									-113	89
B_{42}							-43	$> 10^4$	-298	99
B_{4-2}							-328	$> 10^4$	264	162
B_{43}									-571	126
B_{4-3}									-379	177
B_{44}					-184	1315	-614	$> 10^4$	14	109
B_{4-4}					851	319	-104	$> 10^4$	-63	189
B_{61}									335	112
B_{6-1}									108	148
B_{62}							-640	$> 10^4$	264	151
B_{6-2}							-17	$> 10^4$	59	138
B_{63}									-793	87
B_{6-3}									99	242
B_{64}					-1143	656	-28	$> 10^4$	-79	140
B_{6-4}					423	1764	-118	$> 10^4$	29	318
B_{65}									-38	149
B_{6-5}									-270	166

B_{66}			-1016	$> 10^4$			569	$> 10^4$	148	194
$B_{6\text{-}6}$			-458	$> 10^4$			254	$> 10^4$	-62	171

Table S10. Energies and composition fitted for the KDs of the ground J=15/2 multiplet of **Dy_2**, assuming C_1 symmetry and no coupling. We only reported contributions >1%.

C_1	Energy / cm^{-1}							
	0	191	241	292	332	359	502	653
m_j	$\|1_{CF};\pm\rangle$	$\|2_{CF};\pm\rangle$	$\|3_{CF};\pm\rangle$	$\|4_{CF};\pm\rangle$	$\|5_{CF};\pm\rangle$	$\|6_{CF};\pm\rangle$	$\|7_{CF};\pm\rangle$	$\|8_{CF};\pm\rangle$
+15/2	84%		1%	11%		2%	1%	
+13/2	10%	5%	17%	53%	2%	5%		3%
+11/2	3%	7%	12%	12%	4%	37%	7%	14%
+9/2	3%	17%	12%	4%	7%	2%	14%	28%
+7/2		21%	9%	2%	12%		23%	20%
+5/2		7%	14%	4%	16%	2%	21%	11%
+3/2		8%	21%		11%	25%	10%	12%
+1/2		19%	3%	3%	13%	5%	15%	7%
-1/2		7%	2%	3%	9%	8%	3%	3%
-3/2		2%	1%	1%	8%	1%		1%
-5/2		4%	1%	4%	8%	6%	1%	1%
-7/2		2%	2%		5%	2%	1%	1%
-9/2			3%	2%	3%	4%	1%	
-11/2			1%		2%		1%	
-13/2			1%		1%	1%	1%	
-15/2								

Table S11. CF strength of the calculated CF parameters in C_1 symmetry. We used the following notation: $S_k = \sqrt{\frac{1}{2k+1}(\left|B_k^0\right|^2 + 2 * \sum_{q\neq 0}\left|B_k^q\right|^2)}$ and $S_{tot} = (S_2 + S_4 + S_6)/3$.

	Fit / cm^{-1}
S_2	286
S_4	537
S_6	382
S_t	402

Table S12. Energies and composition fitted for the KDs of the ground J=15/2 multiplet of **Dy_2**, assuming C_{2v} symmetry and no coupling. We only report contributions >1%.

C_{2v}	Energy / cm^{-1}							
	0	191	242	294	333	359	501	653
m_j	$\|1_{CF};\pm\rangle$	$\|2_{CF};\pm\rangle$	$\|3_{CF};\pm\rangle$	$\|4_{CF};\pm\rangle$	$\|5_{CF};\pm\rangle$	$\|6_{CF};\pm\rangle$	$\|7_{CF};\pm\rangle$	$\|8_{CF};\pm\rangle$
+15/2	97%					1%		
+13/2		9%	61%	20%				
+11/2	2%				7%	38%	27%	10%
+9/2		3%	13%	7%				
+7/2					3%	13%	24%	25%
+5/2		15%	3%	31%				
+3/2					36%	8%		14%
+1/2		42%	1%	2%				
-1/2					38%	7%		9%
-3/2		23%	15%	3%				
-5/2					7%	15%	8%	21%
-7/2		7%	6%	22%				
-9/2					4%	14%	38%	20%
-11/2		1%		14%				
-13/2					4%	3%	2%	1%
-15/2				1%				

FIR Comparison

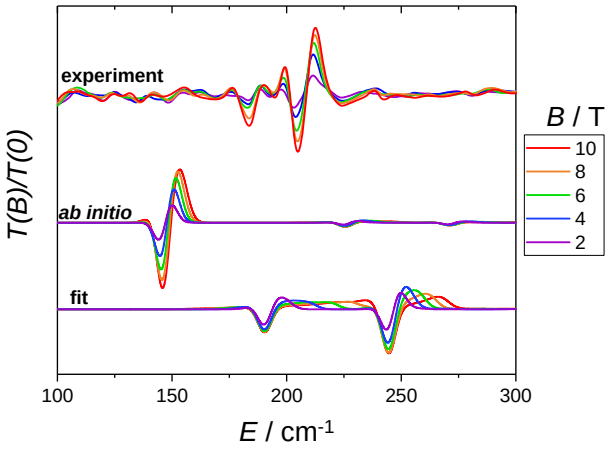

Figure S18. Comparison between the FIR spectra experimentally recorded, simulated using the *ab initio* CF parameters and simulated using the fitted CF parameters.[3]

DC Magnetometry- symmetry comparison

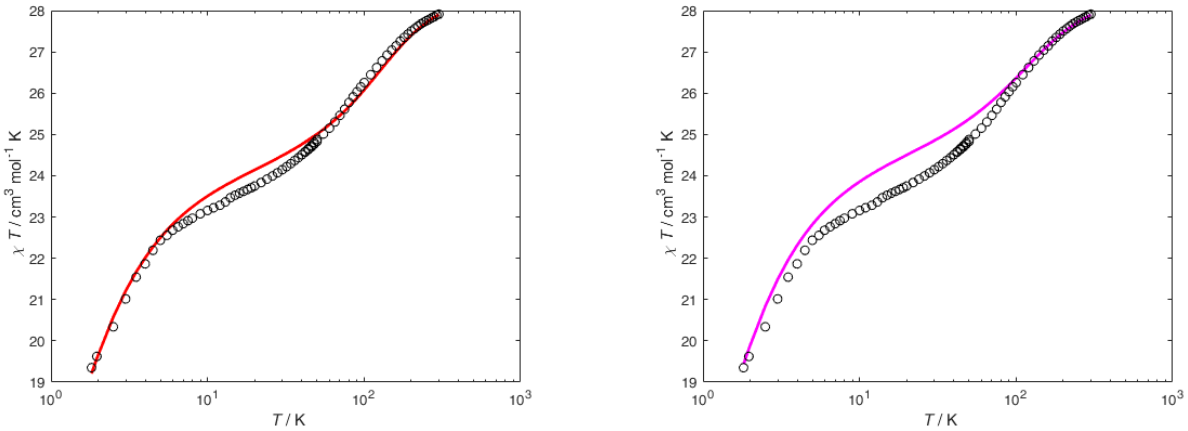

Figure S19 Simulations of χT versus T on the basis of the CF parameters obtained from fits assuming C_1 (red line, left) and C_{2v} (magenta line, right) symmetries. Coupling constant j = 0.042 cm^{-1}.

Cantilever Torque Magnetometry

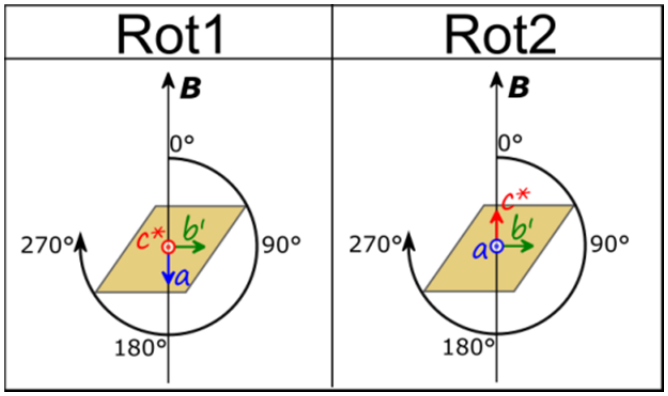

Figure S20. Position of the crystal during Rot1 and Rot2.

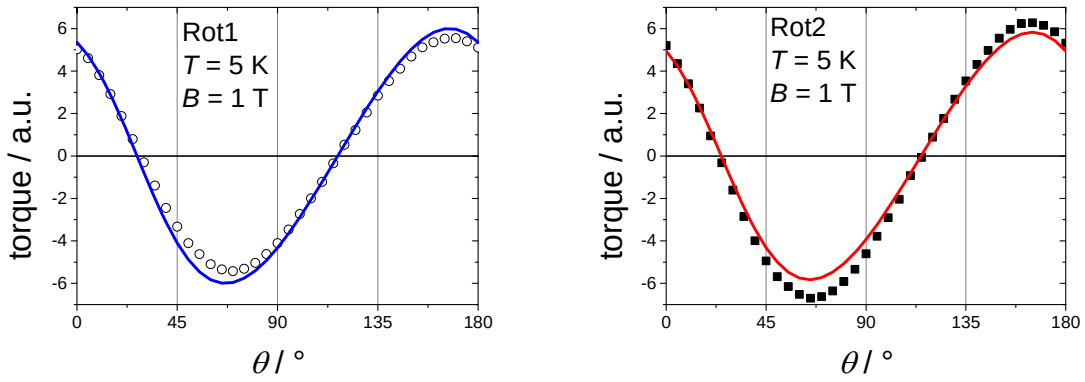

Figure S21. CTM experimental points (symbols) and best fit (lines) for Rot1 (left) and Rot2 (right).

Table S13. Experimental and calculated director cosines of the principal axes of the susceptibility tensor in the Dy_2 crystal. The angles α_1, α_2 and α_3 are the ones between the *x*, *y* and *z* molecular axes and the *a*, *b*' and *c** orthonormal crystallographic axes. The last column of the table represents the discrepancy between experimental and calculated position of the axes.

	$\cos(\alpha_1)$		$\cos(\alpha_2)$		$\cos(\alpha_3)$		$\lvert v_{exp} \cdot v_{calc} \rvert$
	Exp.	Theo.	Exp.	Theo.	Exp.	Theo.	
x	-0.493	-0.023773	-0.371	-0.225321	0.786	0.973994	30°
y	0.772	0.902275	0.229	0.414711	0.593	0.117961	31°
z	-0.400	-0.430505	0.900	0.881615	0.174	0.193443	2°

References

1. S. Alvarez, P. Alemany, D. Casanova, J. Cirera, M. Llunell and D. Avnir, *Coord. Chem. Rev.*, 2005, **249**, 1693-1708.
2. K. S. Cole and R. H. Cole, *The Journal of chemical physics*, 1941, **9**, 341-351.
3. S. Stoll and A. Schweiger, *J. Magn. Reson.*, 2006, **178**, 42-55.